JOURNAL OF APPLIED ELECTROCHEMISTRY 26 (1996) 1045–1052

# Electrochemical behaviour of iron and iron oxide thin films in alkaline (1 M KOH) aqueous solution: a voltammetry study for cathodic instability of coating/metal interface

I. SONG*, D. GERVASIO‡, J. H. PAYER

*Department of Materials Science and Engineering, The Case School of Engineering, Case Western Reserve University, Cleveland, OH 44106-7204, USA*

Received 14 August 1995; revised 20 December 1995

The electrochemical behaviour of thin film metallic iron and the iron oxides in 1 M KOH anaerobic aqueous solution was studied by cyclic voltammetry technique. The material studied was of thin film (50 nm) iron supported on a glass substrate, and the oxide thermally formed on the iron film. The voltammetry of thin film iron on glass was similar to that of low carbon steel and gave a convenient means for preparing specimens for obtaining information relevant to the degradation of structural steel. In this report, the formation of various types of oxides on the iron surface are identified, and the electrochemical stability of the oxides and their relevance to the cathodic disbonding of organic coating from cathodically protected steel pipelines are discussed.

## 1. Introduction

The past few decades have seen numerous reports about the structural, chemical and electrochemical properties of iron and iron oxides in various conditions. A variety of different analytical techniques were utilized to characterize various properties and behaviours of iron and iron oxides. A few examples include X-ray photoelectron spectroscopy [1–3], infrared spectroscopy [4–6], Mossbauer effect spectroscopy [7–9], X-ray absorption spectroscopy [10–12], electron energy loss spectroscopy [13–15], diffraction [16–18] and electrical conductivity measurement [19–21]. In addition to these analytical techniques, voltammetry has been widely used in studying the electrochemical behaviour of the iron and iron oxides in various aqueous environments [22–24]. The results of these voltammetric studies have led to in-depth fundamental understanding of many degradation processes in low carbon steel structures (e.g., pipelines, storage tanks etc.). In the present work, the application of the voltammetry technique has been revisited for characterization of the electrochemical behaviour of iron and thermally formed iron oxides in the form of a film (50 nm). Differing from other works that had used bulk electrodes [22–26], the total amount of the electrode material in the film electrodes used in this study is only approximately 10 $\mu$g on 0.25 $cm^2$. Using the film electrode allows the loss of material to be easily appreciated from visual examinations as well as from changes in the voltammograms during the experiments. In the following, some background of corrosion protection of coated steel pipelines and cathodic disbonding phenomenon is briefly described.

Buried steel pipes are commonly protected from corrosion by covering the outside with an electrically insulating organic coating, and cathodically protecting any steel surface that might remain exposed due to defects in the coating [27]. Disbonding of several organic coatings, such as polybutadiene, has been reported to occur faster when accompanied by cathodic protection than when there is no cathodic protection [28, 29]. The research reported herein is aimed at improving the understanding of the disbonding of organic coatings from cathodically protected pipelines. The information obtained from electrochemical measurements on the surface oxide will serve as a rational basis for evaluation of coating performance and determination of controlling parameters. The understanding of the electrochemical behaviour (e.g., stability of iron oxide at a given pH at different potentials) of iron and iron oxides (especially, thermally formed oxides on the surface of iron) is essential in establishing the mechanism of cathodic disbonding, because coating adhere to oxide, not directly to the substrate steel. Furthermore, since the pipeline steel is under cathodic polarization, electrochemical reactions (e.g., oxygen reduction, oxide reduction etc.) occurring at a cathodic potential can greatly affect the stability of the coating/steel interface, which maintains the integrity of the coating on the steel pipeline.

* Author to whom correspondence should be addressed.
‡ Present address: Redbank Research Co., Redbank, NJ 07701-7040, USA

0021-891X 

In this work, voltammetry of iron film on glass in alkaline aqueous solution was conducted to determine that the iron film on glass exhibits similar voltammetric behaviour as low carbon steel (e.g., ASTM A516 steel) as reported previously under similar conditions [30]. This similarity in voltammetric behaviour of iron film and bulk steel allows the use of thin film iron as specimens in other work, for example, study of iron and iron oxide by X-ray absorption spectroscopy for cathodic disbonding of fusion-bonded epoxy [31]. The results of voltammetry experiments further described how thermally formed iron oxides would behave under electrochemical conditions similar to those used for evaluation of protective coatings.

'Anodic window-opening experiments' were conducted to determine the formation and breakdown of various oxides of iron as a function of potential in alkaline aqueous solution. In the anodic window-opening experiment, the upper limit of the potential cycle is increased stepwise upon completion of each scan cycle, while the lower limit is fixed at the hydrogen evolution potential. In this study, the range of the potential scan (i.e., width of window) was varied from hydrogen evolution (−1.5 V vs SCE) to prepassive potentials (−0.65 V vs SCE) on iron. Hydrogen evolution and oxidation/reduction peak currents were measured to follow the loss of material (metal and/or oxide).

Finally, in order to examine the electrochemical behaviour of thermally formed iron oxides in the electrochemical conditions similar to those of cathodic protection of steel pipelines and those used for coating disbonding tests, voltammetry experiments were performed. Voltammetry of an air-oxidized iron specimen supported on glass established a technical basis for rationalizing the chemical equilibria between thermally formed iron oxides and alkaline aqueous environment.

## 2. Experimental details

### 2.1. *Preparation of thin film iron*

Thin film iron specimens (50 nm, 99.9%) were prepared by magnetron sputtering (Midwest Research Technologies, Brookfield, Wisconsin) onto glass substrates (76 mm × 25 mm × 1 mm, part 2947, Corning Glass Works). Prior to the sputtering of iron, the glass substrates were ultrasonically cleaned with methanol, acetone, and isopropanol for 10 min in each cleaning medium. The substrate was etched with argon at 1100 V pallet voltage, 500 W forward power, for 30 s, at 8 mtorr chamber pressure. The sputter deposition was done at 390 V target voltage, 700 W forward power, for 10 min, at 8 mtorr chamber pressure, and then at 500 V target voltage for 22.5 min. The distance between the iron target and the substrate was set to 7.5 cm. This yielded 50 nm thick continuous iron film on glass substrate. The base pressure for the sputtering process was $1.2 \times 10^{-6}$ torr. The thin film iron specimens were characterized by X-ray photoelectron spectroscopy (XPS, model 5400, Physical Electronics). As shown in Fig. 1, elements found in the specimen as-sputtered condition are iron, oxygen (probably from surface oxide) and carbon (probably from adventitious carbon).

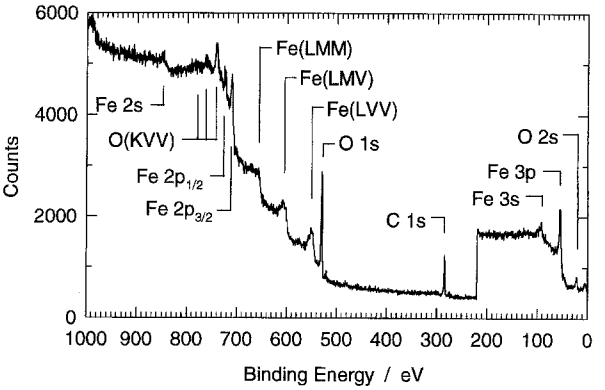


Fig. 1. XPS survey spectrum of the thin film iron specimen in as-deposited condition. (Take-off angle: 20°; Acquisition time: 2.22 min; Mg$K_\alpha$, 400 W).

### 2.2. *Characterization of iron in aqueous solution by voltammetry*

Voltammetry was carried out at room temperature in a three-compartment pyrex cell. A gold counter electrode was used for studies of iron voltammetry. The reference compartment was connected to the main compartment via a Luggin capillary. A saturated calomel electrode was the reference electrode. The reference electrode was placed in a beaker filled with saturated KCl solution which was connected to the reference compartment using a cracked stopcock bridge filled with the same electrolyte as in the specimen (i.e., working electrode) compartment. Additionally, in order to prevent the introduction of chloride species from the reference electrode compartment to the working electrode compartment, the level of the KCl solution in the reference compartment was maintained lower than the electrolyte level in the working electrode compartment. The three-electrode configuration was controlled with a potentiostat (model 173, PAR), a waveform generator (model 175, PAR), and the current–potential data were recorded on an X–Y recorder (Model WX1000, Watanabe).

Iron voltammetry electrodes were an iron film (50 nm) deposited on a glass slide by sputtering. All experiments were carried out in deaerated solutions. The solution was initially deaerated by bubbling nitrogen through the solution and, during the experiment, nitrogen was blanketed over the solution. All experiments were conducted in quiescent solution. Electrical connection to the as-deposited electrode was made using a tin-coated copper alligator clip. Silver paint (type 22-201, GC Electronics) was applied to the contact area to ensure electrical continuity. Teflon tape (type 51520, Fel-pro Inc.) was wrapped around the junction to protect the junction from

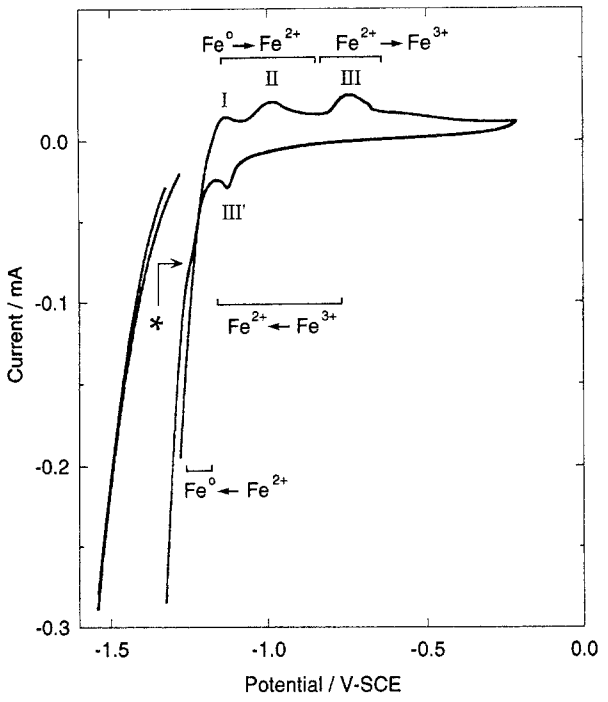


Fig. 2. Cyclic voltammogram of iron (50 nm) on glass after ~20 cycles in aqueous anaerobic 1 M KOH solution (pH 14). Scan rate: 2 mV $s^{-1}$. Room temperature. Electrode area: ~0.25 $cm^2$. The curve shown at potentials more negative than −1250 mV vs SCE is the extension of the cathodic curve on a less sensitive (by a factor of 10) current scale.

solution splash. The contact area was kept above the solution level.

The following pretreatment preceded the voltammogram shown in Fig. 2. The iron on glass electrode was submerged in deaerated 1 M KOH aqueous solution and kept until the change in the open circuit potential (o.c.p.) was less than 1 mV $min^{-1}$. The o.c.p. was −0.7 V vs SCE. Starting at o.c.p., the potential of the electrode was scanned to the negative direction. The electrode was then cycled between −1.5 and −0.2 V vs SCE twenty times; and finally, it was held at −1.5 V vs SCE for about 1 h. Holding at −1.5 V vs SCE resulted in a large negative current, but no hydrogen bubble evolution was visible. The voltammogram shown in Fig. 2 began with the potential scanning to the positive direction after the treatment at −1.5 V vs SCE.

### 2.3. *Anodic window-opening from hydrogen evolution to prepassive potentials on iron*

In these experiments, the upper limit of potential cycle was increased stepwise upon completion of each cycle, while the lower limit was fixed at the hydrogen evolution potential. The voltammograms were taken sequentially with the same specimen used in the previous section. In each case, the iron on glass was first held at −1.5 V vs SCE for 5 min, and the electrode potential was scanned at 2 mV $s^{-1}$. Holding at −1.5 V vs SCE was done in order to bring the electrode surface to the reduced metallic state. Each cycle consisted of a scan in which the electrode potential was swept in the positive (anodic) direction to the anodic limit, then a scan was made in the negative direction back to −1.5 V vs SCE.

### 2.4. *Hydrogen evolution and peak currents to follow metal loss*

The voltammetry was performed with the same electrode used in the previous experiments (anodic window-opening; i.e., the upper limit of potential cycle is increased stepwise upon completion of each cycle, while the lower limit is fixed at the hydrogen evolution potential). This experiment was to examine the possible metal loss as a consequence of the many potential cycles which occurred during the experiments described above. The voltammetry began with the electrode potential scanning in the positive direction after the treatment at −1.5 V vs SCE.

### 2.5. *Voltammetry of air-oxidized iron on glass specimens*

An iron film (50 nm) deposited on a glass substrate was oxidized in air for 8 h at 240 °C. The electrode area was approximately 0.25 $cm^2$. The electrical connections to the electrode were made in the same way as described above. The voltammetry experiment was conducted in aqueous 1 M KOH (pH 14) solution degassed with nitrogen and equilibrated with 1 atm of nitrogen over the solution. The potentiodynamic scan rate was 2 mV $s^{-1}$.

## 3. Results and discussion

### 3.1. *Characterization of iron in aqueous solution by voltammetry*

Figure 2 shows the voltammograms of an iron film (50 nm, area ~0.25 $cm^2$) on a glass substrate in anaerobic aqueous 1 M KOH (pH 14) solution). The features of the voltammogram in Fig. 2 are similar to those reported by Bewick *et al.* [26] for a freshly polished iron electrode obtained under a similar condition. In their work, the bulk iron electrode had been pretreated by holding for 15 min at −1.4 V vs SCE and then holding for a minute more at −1.2 V vs SCE. The initial scan of Fig. 2 began at −1.5 V vs SCE and proceeded in the positive direction at 2 mV $s^{-1}$. The large negative current for water reduction that occurred at −1.5 V vs SCE sharply diminished to lower negative currents as the scan proceeded to more positive potentials. The trace reached zero current at approximately −1.2 V vs SCE. Some oxidation (positive current) waves were seen with the potential proceeding more positive than −1.2 V vs SCE. Shallow peaks (peaks I and II) are visible at approximately −1.15 and −0.95 V vs SCE, and a prominent peak (peak III) occurred at approximately −0.75 V vs SCE. The first oxidation (peak I) of Fe metal to a ferrous state ($HFeO_2^-$) is considered to begin at around −1.15 V vs SCE [26, 30, 32], and this proceeds to the shallow peak (peak II) at −0.95 V vs SCE, which is considered

to be an oxidation to yet another ferrous state, $Fe(OH)_2$ [26, 32, 33]. The oxidation of $Fe(OH)_2$ is considered to occur near −0.75 V vs SCE (peak III) to give principally α-FeOOH as well as the δ and δ′ phases of FeOOH in strongly alkaline solutions [26, 32]. At potentials more positive than the wave peaking at −0.75 V vs SCE, the iron surface appeared to be passivated. This is because iron based metals typically passivate at these potentials at this pH, and in fact no large currents were observed up to the vertex potential, −0.2 V vs SCE. Although the positive direction scan in Fig. 2 was reversed at −0.2 V vs SCE, other voltammograms (not included in this report) indicate that no additional oxidation current would have been seen until the electrode potential was +0.5 V vs SCE. At +0.5 V vs SCE, water is oxidized to molecular oxygen on iron at pH 14.

The negative direction scan in the voltammogram of the iron under nitrogen atmosphere given in Fig. 2 shows oxide reduction ($Fe^{3+} \rightarrow Fe^{2+}$) barely beginning at approximately −0.7 V vs SCE and peaking at −1.1 V vs SCE (peak III′). There is no clear peak for the reduction of $Fe^{2+}$ to metallic iron, but as the scan proceeded to more negative potentials, increasingly large negative currents developed, probably due to both $Fe^{2+}$ reduction as well as water reduction. As the large negative currents developed at potentials more negative than −1.1 V vs SCE, an inflection (feature indicated as *) can be seen at −1.25 V vs SCE, which is at a potential just negative of the crossover of the currents of cathodic and anodic scans. This inflection probably marks the maximum current for reduction of $Fe^{2+}$ to iron metal as the potential was scanned in the negative direction at $2\,mV\,s^{-1}$. A large negative current can be seen at −1.5 V vs SCE at the end of the cycle. This is mainly due to water reduction to molecular hydrogen, although some reduction of $Fe^{2+}$ to iron metal may have been continuing at this potential, as $Fe^{2+}$ reduction apparently is a slow process. Qualitatively, the voltammetry conducted here for iron on glass appears the same as that previously reported for bulk iron by Bewick *et al.* [26], and for a low carbon ASTM A516 steel reported by Payer *et al.* elsewhere [30].

Window-opening experiments (to be discussed below) indicate that in the negative going scan, the peaks for $Fe^{3+}$ reduction at −1.1 V vs SCE (peak III′) and for $Fe^{2+}$ reduction at −1.25 V vs SCE (Inflection*, which appears at a potential just negative of the crossover of the currents of the cathodic and anodic scans) are suppressed if the preceding positive going scan is reversed before reaching −0.8 V vs SCE. Two features useful for monitoring the iron metal electrode area are the hydrogen evolution current at approximately −1.4 V vs SCE and the charge under the peak centred at approximately −0.75 V vs SCE (peak III) corresponding to the oxidation of $Fe^{2+}$ to $Fe^{3+}$. The hydrogen current for Fig. 2 was approximately −1.1 mA at −1.4 V vs SCE, and the charge for the $Fe^{2+}$ oxidation was approximately 1 mC. This charge corresponds to roughly 15 nm of iron oxide on 0.25 $cm^2$ superficial area. As will be shown in a later section, the hydrogen evolution current and the charge of $Fe^{2+}$ oxidation decreased as iron was lost from the glass.

### 3.2. *Anodic window opening from hydrogen evolution to prepassive potentials on iron*

Figure 3(a) shows the voltammogram of the thin iron film on glass in anaerobic aqueous 1 M KOH solution when the potential was cycled from −1.5 to −1.05 V vs SCE. The first feature of the anodic scan shows a large initial current attributed to reduction of water to molecular hydrogen at −1.5 V vs SCE. This current approaches zero as the potential is scanned through −1.2 V vs SCE at $2\,mV\,s^{-1}$. A small anodic peak is seen at approximately −1.5 V vs SCE. This is attributed to the oxidation of iron metal to a $Fe^{2+}$ species. The potential was reversed at −1.05 V vs SCE, and no reduction peaks are evident. The hydrogen current is somewhat diminished on the reversed scan. This is due either to the slower kinetics of water reduction on the oxide versus metal surface, or more likely due to the faster kinetics of hydrogen evolution from the cleaner surface (i.e., oxide-free) that results from holding in the hydrogen region for 5 min.

Figure 3(b) shows the voltammogram for the potential cycle between −1.5 to −0.85 V vs SCE. Two peaks are visible: one at −1.15 V vs SCE (peak I) and another at −0.98 V vs SCE (peak II). The first peak at −1.15 V vs SCE again is attributed to oxidation of metallic iron to one form of $Fe^{2+}$ species, and the second peak is attributed to the oxidation of metallic iron to another form of $Fe^{2+}$ species. No other features are seen except for the initial and final hydrogen current, which are similar to those in the last cycle as explained for Fig. 3(a) above.

Figure 3(c) shows the voltammogram for the potential cycle between −1.5 and −0.75 V vs SCE. The features seen in Fig. 3(a) and (b) are present, plus two new features: a rising anodic (positive) current at the upper limit, −0.75 V vs SCE, and a shallow cathodic (negative) peak at −1.05 V vs SCE (peak III′). The rising anodic current at −0.75 V vs SCE marks the onset of $Fe^{2+}$ to $Fe^{3+}$, and the shallow cathodic peak at −1.05 V vs SCE (peak III′) is the reduction of $Fe^{3+}$ back to $Fe^{2+}$.

Figure 3(d) shows the voltammogram for the potential cycle between −1.5 and −0.65 V vs SCE. The number of features are the same as in Fig. 3(c) above. In Fig. 3(d), the oxidation of $Fe^{2+}$ to $Fe^{3+}$ shows a clear peak at −0.72 V vs SCE (peak III), and the reduction of $Fe^{3+}$ to $Fe^{2+}$ is more pronounced at peaks at −1.1 V vs SCE (peak III′). Figure 3(e) shows the voltammogram for the potential cycle between −1.5 and −0.55 V vs SCE. This voltammogram is essentially the same as Fig. 3(d) above. Probably due to longer time needed to reduce the greater amount of oxide that formed when the upper limit was −0.55 V vs SCE instead of −0.65 V vs SCE, the peak for $Fe^{2+}$ oxidation to $Fe^{3+}$ (peak III) appears at −0.74 V vs SCE instead of −0.72 V vs SCE.

### 3.3 *Hydrogen evolution and peak currents to follow metal loss*

As mentioned above, two voltammetric features useful for monitoring the area of the iron metal electrode are the hydrogen evolution current and the charge under the peak centred at approximately −0.74 V vs SCE (peak III). This peak centred at approximately −0.74 V vs SCE corresponds to the oxidation of $Fe^{2+}$ to $Fe^{3+}$. These two features can be observed in Fig. 2. The hydrogen current at −1.5 V vs SCE was approximately −1.1 mA. The charge for the $Fe^{2+}$ oxidation to $Fe^{3+}$ in the wave centred around the peak at −0.74 V vs SCE (peak III) was approximately 1 mC. This charge corresponds to the formation of roughly 15 nm thick iron ($Fe^{3+}$) oxide on 0.25 $cm^2$ of projected area without considering surface roughness.

Figure 4 shows the hydrogen current taken immediately after preconditioning the electrode by holding at −1.5 V vs SCE for 1 h, that is, in the same way as was done before taking the voltammogram in Fig. 2. The voltammogram shown in Fig. 4 was taken after the electrode was cycled many times since it was used to give the voltammogram shown in Fig. 2. The hydrogen evolution current at −1.5 V vs SCE shown in Fig. 4 is approximately 0.4 mA, which is about half that shown in Fig. 2. This suggests that about half the metal area was lost as a result of the many potential cycles taken between the recording of Figs 2 and 4. Similarly, in Fig. 4, the charge for the oxidation of $Fe^{2+}$ to $Fe^{3+}$ (peak III) was about 0.6 mC, which is about 60% of the charge for this process for the voltammogram shown in Fig. 2. This loss of surface oxidation charge suggests that about 60% of the area was lost from the electrode due to the potential cycling done between the time Figs 2 and 4 were taken. The comparison of the hydrogen currents before and after cycling indicate around 50% of the area was lost, and the oxide peaks before and after cycling indicate around 60% of the area was lost. That these two area-dependent criteria are in good qualitative agreement gives a good indication that cycling did lead to a loss of electrode area, which probably is the direct consequence of the loss of metal. The loss of metal was also visually observed. With 50 nm iron on glass, the specimen was a uniform metallic grey, but after the cycling experiment the specimen showed some areas that became transparent (i.e., only glass substrate remained).

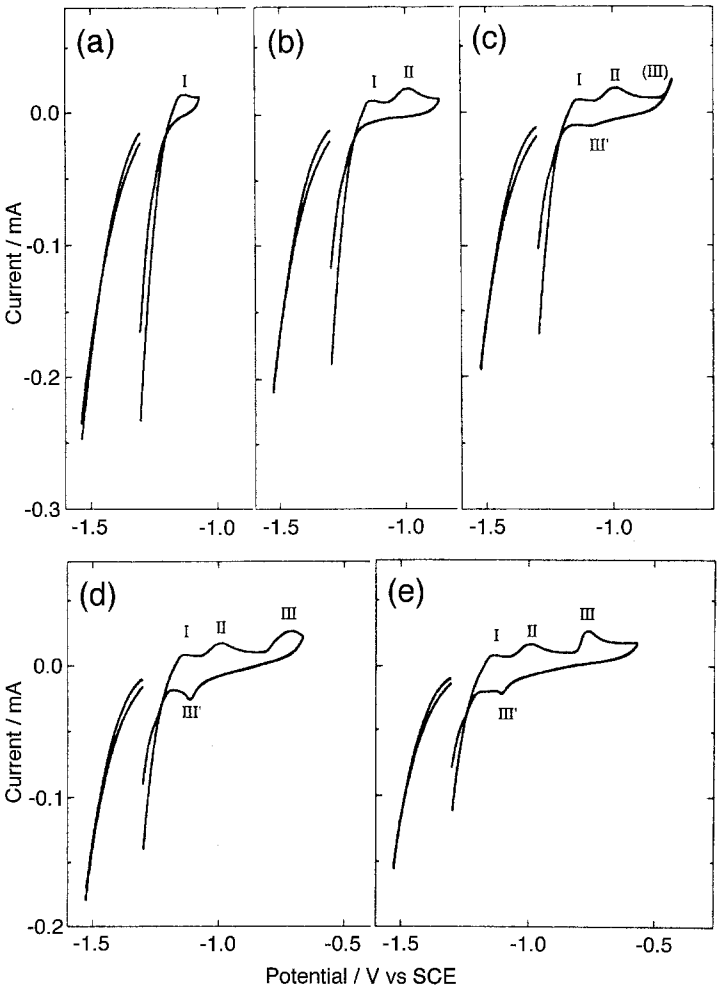


Fig. 3. Cyclic voltammograms of iron (50 nm) on glass in aqueous anaerobic 1 M KOH solution (pH 14). Scan rate: 2 mV $s^{-1}$. Room temperature. Electrode area: ~0.25 $cm^2$. The curve shown at potentials more negative than −1275 mV vs SCE is the extension of the cathodic curve on a less sensitive (by a factor of 10) current scale. (a) Cycled from −1.5 to −1.05 V vs SCE; (b) cycled from −1.5 to −0.85 V vs SCE; (c) cycled from −1.5 to −0.75 V vs SCE; (d) cycled from −1.5 to −0.65 V vs SCE; (e) cycled from −1.5 to −0.55 V vs SCE.

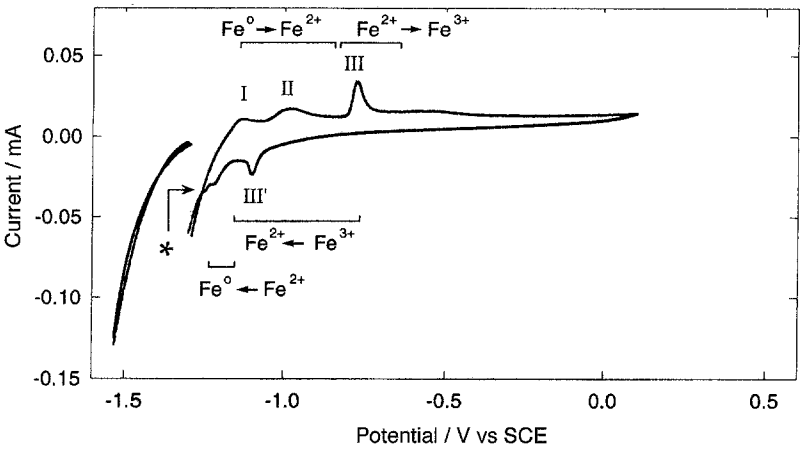


Fig. 4. Cyclic voltammogram of iron (50 nm) on glass in aqueous anaerobic 1 M KOH solution (pH 14). Scan rate: 2 mV $s^{-1}$. Room temperature. Electrode area: ~0.25 $cm^2$. The curve shown at potentials more negative than −1275 mV vs SCE is the extension of the cathodic curve on a less sensitive (by a factor of 10) current scale.

### 3.4. *Voltammetry of air-oxidized iron on glass specimens*

Figure 5(a) shows the first few cycles of the voltammograms of the iron oxide specimen that had been formed thermally on the iron-deposited glass. The scan was started at the open circuit potential (−0.72 V vs SCE) and cycled in the negative direction. The cathodic (lower) limit was increased after each

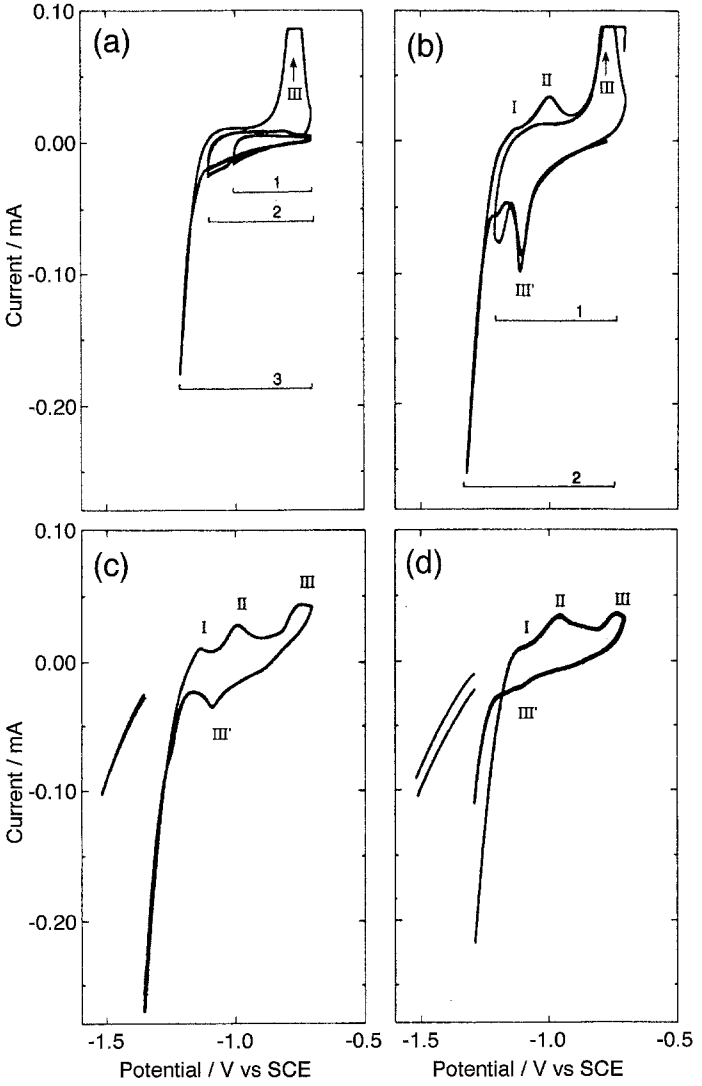


Fig. 5. Cyclic voltammogram of iron (50 nm) oxidized in air for 8 h at 240 °C on glass in aqueous anaerobic 1 M KOH solution (pH 14). Scan rate: 2 mv $s^{-1}$. Room temperature. Electrode area: ~0.25 $cm^2$. Horizontal bars with numbers indicate the cycling range and sequence. (a) Cycled 1. between −0.72 and −1.0, 2. between −0.72 and −1.1, and 3, between −0.72 and −1.2 V vs SCE; (b) 1. between −0.72 and −1.2, and 2. −0.72 and −1.3 V vs SCE; (c) between −0.72 and −1.5 V vs SCE; (d) between −0.72 and −1.5 V vs SCE, taken 14 hours after the voltammogram (c) was taken. In (a) and (b), the flat top of the ferric oxide peak is due to reaching the limit of recorder span.

cycle. The first cathodic limit was −1, then −1.1 and then −1.2 V vs SCE. There was no significant oxide reduction or reoxidation when the cathodic limit was as low as −1.1 V vs SCE. Upon reaching the cathodic (i.e., lower) limit of −1.2 V vs SCE, a pronounced reduction current was found, corresponding to the reduction of $Fe^{3+}$ to $Fe^{2+}$, followed by water reduction to molecular hydrogen. On the reverse scan of this cycle, a pronounced oxidation wave (peak III) was seen for the first time. The peak centred at approximately −0.8 V vs SCE corresponds to the reoxidation of $Fe^{2+}$ to $Fe^{3+}$.

Figure 5(b) shows the continued cathodic window opening from −1.2 to −1.3 V vs SCE. As indicated in other reports conducted in similar conditions [26, 30, 32], and as predicted by potential–pH diagram [33], only the $Fe^{2+}$ and $Fe^{3+}$ valencies of iron oxides are involved in the voltammogram when the lower limit is no more negative than −1.2 V vs SCE. When the lower limit is extended to −1.3 V vs SCE a peak is found at approximately −1.2 V vs SCE (feature *) which probably involves the conversion of a $Fe^{2+}$ to metallic iron, and a large cathodic current is found at the lower limit, which probably involves both the conversion of $Fe^{2+}$ to iron metal and the reduction of water to yield molecular hydrogen and hydroxide ions. Upon reversing the potential scan at the cathodic limit of −1.3 V vs SCE toward the anodic (positive) scan direction, two new peaks at approximately −1.15 and −1.0 V vs SCE are seen for the first time. These probably involve the conversion of iron metal to two different types of $Fe^{2+}$ species as was seen during the anodic scan in this potential region for metal electrodes (e.g., in Figs 2 and 3(b)). However, positive identification of the formation of two $Fe^{2+}$ (insoluble $Fe(OH)_2$; and soluble $HFeO_2^-$), species requires a spectroscopic confirmation, or electrochemical measurements with mass transfer control.

Figure 5(c) shows the voltammogram of continued cathodic window opening for the thermally oxidized iron specimen after many cycles with extended lower limit to −1.5 V vs SCE. The features are qualitatively similar to those seen in Fig. 5(b) above. One noteworthy observation is that after the many cycles (approximately 10 cycles) taken between Fig. 5(a) and (c), the peak currents have diminished. This rapidly diminishing current appears to be due to loss of electrode area (i.e., loss of material) as it was visually confirmed that some parts of the electrode became transparent, revealing the transparent glass substrate. Thus, the rapidly diminishing current is considered to be due to rapid loss of electrode area, which is the direct consequence of the loss of material from the parts of the electrode. With thermally oxidized iron on glass, the specimen was uniformly yellow in colour, but after the cycling experiment the specimen showed some areas that became transparent (i.e., only glass substrate remained). Further study is required to confirm the oxide breakdown process. Other processes resulting in oxide loss are possible. For example, an alternative, although a less likely, explanation can be offered; that is, the oxide could be converting to a porous metal, which then is slow to reoxidize during the cycling process due to distributed impedance effects, as is often seen in porous gas-fed electrodes.

Figure 5(d) is the voltammogram of the specimen taken after that shown in Fig. 5(c). The specimen was kept polarized at −1.5 V vs SCE for 14 h during the time between the voltammograms shown in Fig. 5(c) and (d) were measured. These voltammograms were obtained under the same condition, and their characteristics are virtually the same. This indicates that holding at −1.5 V vs SCE alone is not enough to lead to the oxide breakdown and/or the loss of material that were observed from cycling the potential to −1.5 V vs SCE; that is, cycling between some higher potential (e.g., −1 V vs SCE) and −1.5 V vs SCE causes more effect of oxide breakdown and/or loss of material than holding the electrode potential constant at −1.5 V vs SCE.

To recapitulate, oxide breakdown seems to come about from potential cycling to −1.5 V vs SCE, but not holding at −1.5 V vs SCE. This is surprising, but seems to agree with what is anticipated from the potential–pH diagram of iron. The potential–pH diagram predicts that there exists a region in which neither metallic nor oxide iron is stable as insoluble solid form. Providing that the pH remains constant throughout an experiment, a linear sweep voltammogram, in a coarse sense, represents merely the vertical cut at a constant pH. From the potential–pH diagram it is apparent that at pH 14, iron dissolves into solution as ferrous state ($HFeO_2^-$) at potentials near −1.15 V vs SCE [33]. Thus, for this work done at pH 14, it is reasonable to state that the specimens experienced the condition in which dissolved ferrous state ($HFeO_2^-$) is more stable than solid state ($Fe(OH)_2$ or Fe) when the electrode potential passes through −1.15 V vs SCE during cycling, and the solid species (metallic and/or oxidic iron) dissolved into the solution. The kinetics of the dissolution of solid at −1.15 V vs SCE and the stability of oxide at −1.5 V vs SCE are not obvious with the present data. However, the data indirectly suggests that one possible route to the disbonding of coating from steel pipeline may be due to the dissolution of solid species at the coating/oxide/steel interfaces.

### 3.5. *Relevance to cathodic disbonding of pipeline coatings*

In summary, the results of this study are in agreement with that predicted by the electrochemical equilibria of iron in aqueous electrolyte [33]. The potential–pH diagram, often referred to as a Pourbaix diagram, of iron has several regions where iron exists as soluble species. One of the regions is in alkaline pH (roughly, higher than pH 13) and near −1.15 V vs SCE. In that region, iron is stable in the form of dihypoferrite, $HFeO_2^-$, as soluble species. The metallic iron or iron oxides can dissolve into solution when the condition is met. Thus, a similar situation may arise in the

cathodically protected underground pipelines. Underground pipelines are generally protected from corrosion by the application of a cathodic potential. The cathodic protection level is recommended to be lower (i.e., more negative) than −0.85 V vs $Cu/CuSO_4$ (equivalent to −0.78 V vs SCE), but actual potential of the pipeline under cathodic protection can vary in a wide range of potential and can easily reach to −1.5 V vs SCE or even lower depending of the conditions of soil, coating and the geometry of anode placement. Similar situation is found in many standard accelerated tests for coating evaluations, where the cathodic polarization is prescribed to −3 V vs $Cu/CuSO_4$ (equivalent to −2.93 V vs SCE). [34, 35] At these cathodic potentials, the pH of electrolyte in the vicinity of the pipeline may increase toward more alkaline conditions either or both by oxygen reduction and/or by water reduction. If the pH approaches to a value higher than 13, the fluctuation of the cathodic protection can make solid species (e.g., passive iron oxide) unstable, and the solid species will dissolve into the ground water as a soluble species (e.g., $HFeO_2^-$). Obtaining such a high pH environment is conceivable, because the volume of electrolyte in the crevice between disbonded coating and pipeline can be considered small. An electrochemical process such as water reduction can greatly affect the chemistry (especially, pH) of the small volume electrolyte. Thus, it is important to mention that excessive cathodic protection may produce an electrochemical environment in which the coating on a steel pipeline may disbond due to instability of metal and/or oxide at the coating/pipeline interface.

## 4. Conclusions

The electrochemical behaviour of metallic iron and the iron oxides in 1 M KOH anaerobic aqueous solution was studied by cyclic voltammetry technique. The voltammetry of thin film (50 nm) iron on glass in anaerobic 1 M KOH aqueous solution was similar to that of low carbon steel and gave a convenient means for preparing specimens for obtaining information relevant to the degradation of structural steel. The voltammetry of thin film iron provided a means for identifying various types of oxides on the iron surface, and monitoring their stability. The cycling of the electrode potential (between −1.3 and −0.72 V vs SCE) resulted in a rapid loss of material from the thin film electrode, and the loss of material was visually observed. The loss of material is attributed to the formation of soluble $HFeO_2^-$ during cycling through the region where $HFeO_2^-$ is stable with respect to iron and the iron oxides. The variation of potential (i.e., temporal fluctuation of the potential at cathodically protected pipelines) at high alkaline environment causes a chemical and possibly structural change in the passive oxide that can lead to an instability of the coating/steel interface.

## Acknowledgements

The authors acknowledge the support of the Gas Research Institute (contract 5091-260-2110) and Dr Kevin Krist of the Basic Research Group at the GRI.

## References

[1] Y. Baer, P. F. Heden, J. Hedman, M. Klasson, C. Nordling and K. Siegbahn, *Physica Scripta* **1** (1970) 55.
[2] N. S. McIntyre and D. G. Zetaruk, *Anal. Chem.* **49** (1977) 1521.
[3] E. McCafferty, M. K. Bernett and J. S. Murday, *Corr. Sci.* **28** (1988) 559.
[4] R. Jasinski and A. Iob, *J. Electrochem. Soc.* **135** (1988) 551.
[5] H. Neugebauer, A. Moser, P. Strecha and A. Neckel, *ibid.* **137** (1990) 1472.
[6] A. Bewick, M. Kalaji and G. Larramona, *J. Electroanal. Chem.* **318** (1991) 207.
[7] G. W. Simmons, E. Kellerman and H. Leidheiser, Jr., *Corrosion* **29** (1973) 227.
[8] T. Kanzaki and T. Katsura, *J. Chem. Soc. Dalton Trans.* (1986) 1243.
[9] J. F. Marco, J. Davalos, M. Gracia and J. R. Gancedo, *Hyperfine Interactions* **83** (1994) 111.
[10] G. A. Waychunas, M. J. Apted and G. E. Brown, Jr., *Phys. Chem. Minerals* **10** (1983) 1.
[11] A. Manceau and J. M. Combes, *ibid.* **15** (1988) 283.
[12] G. Drager, R. Frahm, G. Materlik and O. Brummer, *Phys. Sat. Sol. B* **146** (1988) 287.
[13] O. L. Krivanek and J. H. Paterson, *Ultramicroscopy* **32** (1990) 313.
[14] J. H. Paterson and O. L. Krivanek, *ibid.* **32** (1990) 319.
[15] C. Colliex, T. Manoubi and C. Ortiz, *Phys. Rev. B* **44** (1991) 11402.
[16] L. Pauling and S. B. Hendricks, *J. Am. Chem. Soc.* **47** (1925) 781.
[17] E. J. Fasiska, *Corr. Sci.* **7** (1967) 833.
[18] C. Greaves, *J. Solid State Chem.* **49** (1983) 325.
[19] E. J. W. Verwey, P. W. Haaijaman and F. C. Romeijn, *Philips Res. Rep.* **5** (1950) 173.
[20] F. J. Morin, *Phys. Rev.* **83** (1951) 1005.
[21] A. K. Nikumbh, K. S. Rane and A. J. Mukhedkar, *J. Mat. Sci.* **17** (1982) 2503.
[22] D. Geana, A. A. El Miligy and W. J. Lorenz, *J. Appl. Electrochem.* **4** (1974) 337.
[23] V. S. Muralidharaan and M. Veerashanmugamani, *ibid.* **15** (1985) 675.
[24] B. Muller-Zulow, S. Kipp, R. Lacmann and M. A. Schneeweiss, *Surf. Sci.* **311** (1994) 153.
[25] H. S. Wroblowa and S. B. Qaderi, *J. Electroanal. Chem.* **279** (1990) 231.
[26] A. Bewick, M. Kalaji and G. Larramona, *ibid.* **318** (1991) 207.
[27] D. P. Werner, S. J. Lukezich, J. R. Hancock and B. C. Yen, presented at Corrosion/92, paper number 366, National Association of Corrosion Engineers, Houston, TX (1992).
[28] H. Leidheiser and W. Wang, *J. Coatings Technol.* **53**(672) (1981) 77.
[29] J. F. Watts and J. E. Castle, *J. Mater. Sci.* **18** (1983) 2987,
[30] J. H. Payer, B. Trautman and D. Gervasio, *in* 'Proc. Polymeric Materials and Engineering', Vol. 68 (edited by D. R. Bauer), Am. Chem. Soc., Denver, CO (1993), pp. 109–110.
[31] I. Song, M. R. Antonio and J. H. Payer, *J. Electrochem. Soc.* **142** (1995) 2219.
[32] W. Tschinkel, H. Neugebauer and A. Neckel, *ibid.* **137** (1990) 1475.
[33] M. Pourbaix, 'Atlas of Electrochemical Equilibria in Aqueous Solutions', National Association of Corrosion Engineers, Cebelcor, Brussels (1974), pp. 307–321.
[34] American Standard for Testing Materials, ASTM G-8 (1985), pp. 895–902.
[35] American Standard for Testing Materials, ASTM G-95 (1987), pp. 995–999.